Original Paper

Influence of filler characteristics on particle removal in fluid catalytic cracking slurry under an alternating electric field

Qiang Li [*], Hui-Zhen Yang , Can Yang , Qing-Zhu Qiu , Wei-Wei Xu , Zhao-Zeng Liu

College of New Energy, China University of Petroleum (East China), Qingdao, 266580, Shandong, China

A B S T R A C T

The characteristics of the packing material under an alternating electric field are an important factor in the removal of FCCS particles. In this study, the electric field distribution of a separation unit consisting of packed spheres under an alternating electric field is simulated, and the movement mechanism of catalyst particles is analysed. An "effective contact point" model is derived to predict the adsorption of filler contact points on catalyst particles under the alternating electric field, and the model is validated by simulations and experiments. The numerical calculation and experimental results indicate that the electrical properties of the filler spheres, the filler angle θ, and the frequency f of the alternating electric field affect the adsorption of catalyst particles. As the frequency of the electric field increases, the particle removal efficiency of the high-conductivity filler (silicon carbide) increases and then settles, and the separation efficiency of the low-conductivity filler (glass, zirconia) is not sensitive to the change in electric field frequency.

1. Introduction

FCCS (fluid catalytic cracking slurry) is a major byproduct of FCC and can be used for secondary processing to produce products such as carbon black, petroleum coke and carbon fibre (Guo et al., 2014; Li et al., 2016; Lou et al., 2021) upon removal of the contained catalyst particles which constrain the subsequent utilization of the slurry (Cui et al., 2020). These catalyst particles are particularly suitable for separation using DEP (dieelectrophoresis) due to their micron diameter, low concentration, and favourable liquid phase insulation (Lin and Benguigui, 1982; Mazumder et al., 2005; Wu et al., 2020). DEP technology makes use of a nonuniform electric field to polarize neutral particles, and particles move under the action of dielectric electrophoresis force in the direction of electric field strength change, thus achieving the effect of manipulating particles (Aldaeus et al., 2006; Adekanmbi et al., 2020; Murugesan and Park, 2017). The electrorheological (ER) effect produced by an applied electric field on a soft material also alters its rheological properties (viscosity, shear stress, etc.), thus affecting the manipulation of the particles (Kuznetsov et al., 2022; Liang et al., 2022).

Xie et al. (2023a, 2023b, 2023c) found that applying an electric field to crude oil causes colloidal particles to move, collide with wax particles and adhere to the surface, which reduces the mutual attraction of the wax particles and significantly improves their cold flowability. They further found that shear destroys the connections between colloidal particles and wax particles and promotes collisions of free colloidal particles and wax particles and that the competing results of the two opposing effects determine the effect of shear on the viscosity of crude oil.

DEP separators for solid-liquid separation usually require the addition of fillers polarized under an electric field to create areas of high electric field strength, thereby moving the particles to specific areas to achieve separation (Lewpiriyawong et al., 2017; Sano et al., 2012). DEP can be divided into DC-DEP and AC-DEP according to the applied electric field. There are many studies on the characteristics of the filler for particle removal of FCCS under a DC electric field. Petrolite Corporation (1980) found that under a direct current field, the filler adsorbed metal residues in the FCCS, increasing the current in the device and causing a short circuit. Gulf Research & Development Company (1975) found that the composition of the glass filler affected the separation efficiency, with glass fillers containing a small amount of potassium oxide outperforming those containing only sodium oxide. Fang et al. (1998) conducted experiments on the removal of FCCS particles under a DC electric field

using a DEP separator and proposed a corresponding "point adsorption" theory, finding that the main adsorption area of the particles being the packing contact point. Li et al. (2020a, 2020b) found that the relationship between the included angle of the filler and the electric field strength at the contact point of the filler is nonlinear and inverse and calculated the model of the size of the filler adsorption area.

Few studies have been conducted on particle removal in FCCS under an alternating electric field. Chevron Research Company (1979) connected AC power to the separator and found that the oscillating electric field can reduce the viscosity of the oil slurry, thus improving the subsequent separation efficiency. Lin and Benguigui (1981) found that the particle removal of FCCS under an alternating electric field can effectively avoid the short circuit of the device caused by the bridging of particles in the separation area. Therefore, it is important to investigate the effect of packing characteristics on FCCS particle removal under an alternating electric field. Here, the electrostatic (es) module and the fluid-particle tracking (fpt) module in COMSOL Multiphysics are used to obtain the electric field strength, the motion of the particles, and the dielectric swimming force applied to a separation cell. Macroscopic and microscopic experiments considering the removal of particles from FCCS under an alternating electric field were conducted using a homemade separator. An "effective contact point" model is developed as a mathematical description of the above experimental and simulation results. The model is dominated by the electrical properties of the filler, the angle of the filler and the frequency of the electric field. This model enables the guidance of filler type selection for the removal of particles from the FCCS under an alternating electric field.

2. Experimental setup and model description

2.1. Experimental device and setup

To conduct the macroscopic experiments, equipment is used as shown in Fig. 1 including an AC power supply, separator, and transformer. The outer shell of the separator is made of transparent organic glass with favourable insulating properties. The outer cylinder of the separator is inserted with a copper strip as the outer electrode; the inner electrode of the device is a copper rod of 8 mm diameter threaded into the upper-end cap of the electrostatic separator. In the annular column space between the inner and outer electrodes, spherical fillers with a diameter of 3 mm are used

to fill the space to a certain height. These fillers can form mutual contact points to adsorb catalyst particles and shorten the distance of particle movement.

Heat-conducting oil homogeneously mixed with catalyst particles was used instead of FCCS because of their similar dielectric constants, conductivity, and favourable flow and insulation properties at room temperature (Cao et al., 2011). In addition, the transparent color of the heat transfer oil makes it easy to observe the adsorption of particles during microscopic experiments. The main component of the catalyst is aluminum silicate ($Al_2O_3 \cdot SiO_2$) with the appearance of black powder and the parameters are shown in Table 1.

Macroscopic experiments on particle removal from FCCS were conducted in three steps.

(1) The batching module, consisting mainly of an analytical balance and an electric stirrer for mixing heat transfer oil and catalyst particles for 30 min to prepare a mixture with a mass concentration of c_0.
(2) The separation module, consisting mainly of an AC power supply, separator and transformer, all three connected by wires. The glass fillers are polarized to produce a local high electric field intensity electric field to drive the solid particles in the mixture. The mass of the mixture obtained after 30 min of separation is m_1.
(3) The analysis module, consisting mainly of a sand core filtration unit, a Soxhlet extraction unit and a vacuum drying chamber. The sand core filter device is used to extract the mixed liquid to obtain the filter paper containing particles, and the Soxhlet extraction device is used to remove the oil phase impurities of the filter paper containing particles. The weight of the filter paper containing particles is m_2.

This experiment uses the mass method to determine the separation efficiency η, as shown in Eq. (1)

Table 1
Catalyst parameters.

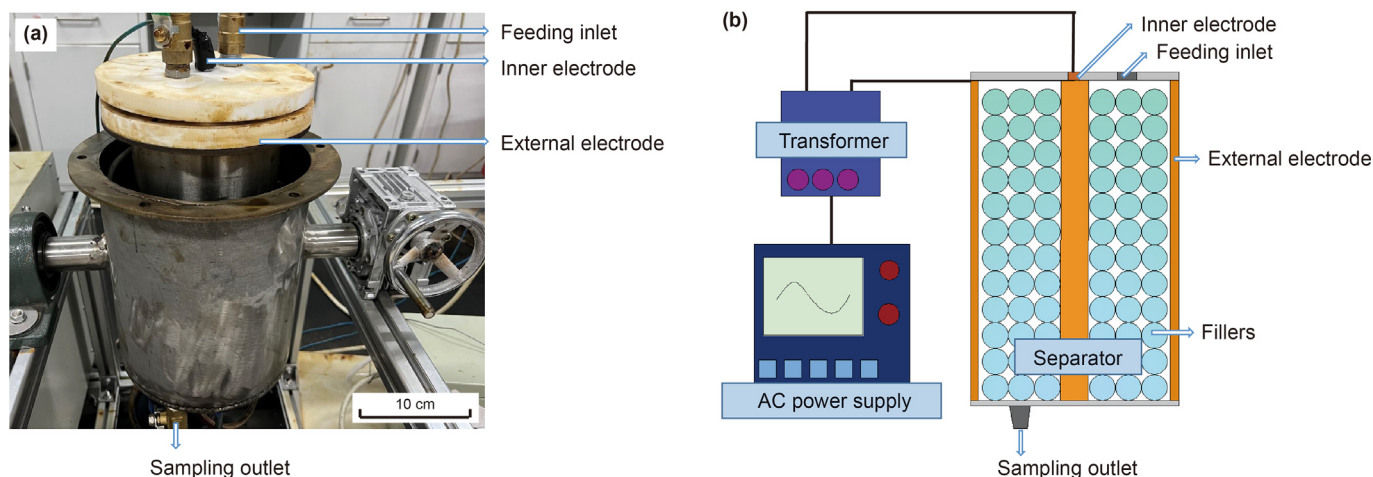| Average diameter, μm	Mid-diameter, μm	Relative dielectric constants
5.07	3.02	6.22

Fig. 1. (a) Separator; (b) Sketch of the equipment.

$$\eta = \frac{c_0 - (m_2 - m_3)/m_1}{c_0} \times 100\% \tag{1}$$

where m_3 is the mass of empty filter paper.

The microscopic experiments for catalyst particle removal were performed using a homemade micro separator and microscope. As shown in Fig. 2, the micro separator was placed on the stage of the microscope to observe the adsorption of particles.

2.2. Model description

Because the separation area of the DEP separator is a symmetrical structure, only a fan ring-shaped calculation area is considered to simplify the calculation. The calculation model and boundary conditions are shown in Fig. 3.

In this study, the effect of the interaction forces between the particles was neglected due to the low catalyst concentration in the mixture. The channel gap formed between fillers is at the millimetre level, AC electroosmosis is neglected, the electrode spacing is large, and there is no electrode array, so the travelling wave dielectric electrophoresis force is neglected. The forces in the final calculation include dielectrophoretic forces F_{DEP}, effective gravity F_G, and Stokes resistance F_{SD}, as shown in Eq. (2).
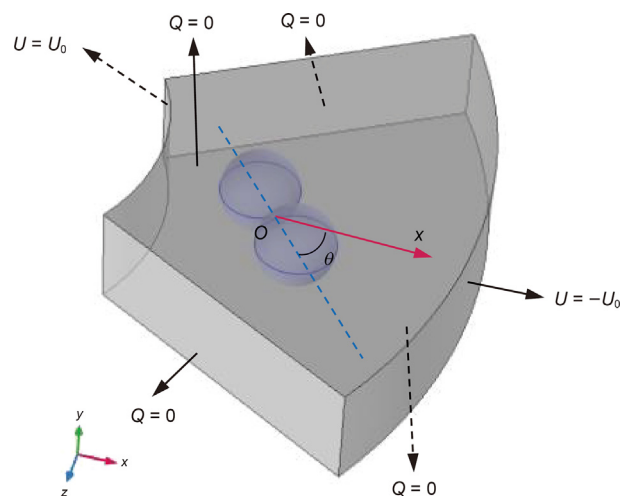

Fig. 3. Schematic diagram of the geometric model and boundary conditions. (U_0 is the applied AC power excitation, and its amplitude is chosen as half of the actual voltage value; Q is the initial charge; θ is the angle between the centre of the two filler balls and the x-axis. During the change in θ, the position of the contact point O (origin of coordinates) of the two fillers remains unchanged.).
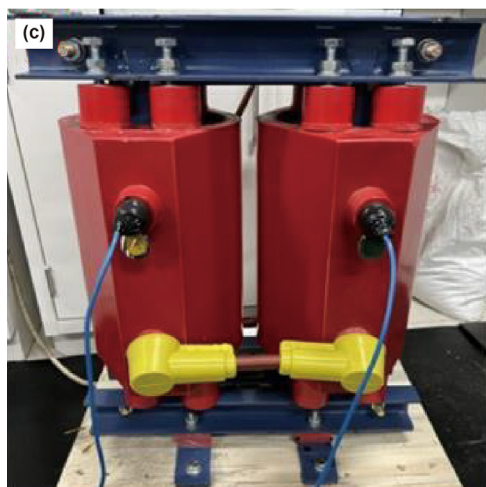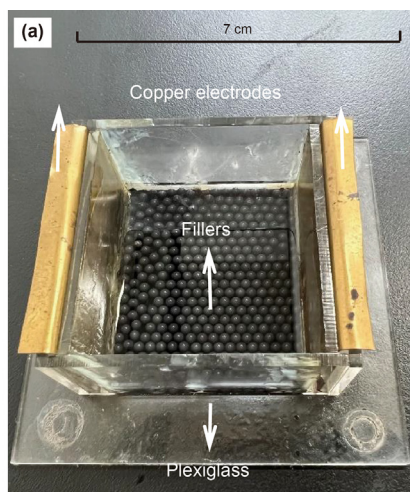

Fig. 2. **(a)** Microscopic separator for catalyst particle removal; **(b)** Microscopic experiments; **(c)** Dry-type power transformer; **(d)** AC programmable power supply.

$$m_{\mathrm{p}}\frac{\mathrm{d}u}{\mathrm{d}t} = F_{\mathrm{SD}} + F_{\mathrm{G}} + F_{\mathrm{DEP}} \tag{2}$$

where m_{p} is the mass of the particle and u is the velocity of the particle.

Assuming a uniform spherical shape with a diameter d_{p} of the catalyst particles, the expression for the dipole moment in an AC field is Eq. (3).

$$P = \frac{1}{2}\pi\varepsilon_{\mathrm{f}}\left(\frac{\varepsilon_{\mathrm{p}}^* - \varepsilon_{\mathrm{f}}^*}{\varepsilon_{\mathrm{p}}^* + 2\varepsilon_{\mathrm{f}}^*}\right)d_{\mathrm{p}}^3 E \tag{3}$$

The dielectrophoretic force on the catalyst particles in the heat conducting oil under the action of the electric field can be expressed as Eq. (4).

$$F_{\mathrm{DEP}} = \frac{\pi}{4}d_{\mathrm{p}}^3\varepsilon_{\mathrm{f}}\mathrm{Re}[f_{\mathrm{CM}}(w)]\nabla|E|^2 \tag{4}$$

where ε_{f} is the dielectric constant of the heat conducting oil. $f_{\mathrm{CM}}(w)$ is the polarization factor (Clausius-Mossotti factor), which can be used to represent the degree of polarization of the particles in the electric field or the magnitude of the dipole moment generated by the polarization of the particles, as shown in Eq. (5).

$$f_{\mathrm{CM}}(w) = \frac{\varepsilon_{\mathrm{p}}^* - \varepsilon_{\mathrm{f}}^*}{\varepsilon_{\mathrm{p}}^* + 2\varepsilon_{\mathrm{f}}^*} \tag{5}$$

In an alternating electric field, the dielectric constant of a substance is shown as Eq. (6).

$$\varepsilon^* = \varepsilon - \mathrm{i}\frac{\sigma}{w} \tag{6}$$

where ε^* and ε denote the composite dielectric constant and dielectric constant of the substance, respectively, and the subscripts p and f denote the catalyst particles and thermal oil, respectively, F/m; σ denotes the electrical conductivity of the substance, S/m; w denotes the angular frequency of the applied alternating electric field, $w = 2\pi f$, Hz; and i denotes the imaginary units, $\mathrm{i} = \sqrt{-1}$.

In Eq. (4), $\mathrm{Re}[f_{\mathrm{CM}}(w)]$ denotes the real part of the CM factor, and substituting Eq. (6) yields Eq. (7).

$$\begin{aligned}\mathrm{Re}[f_{\mathrm{CM}}(w)] &= \mathrm{Re}\left(\frac{\varepsilon_{\mathrm{p}}^* - \varepsilon_{\mathrm{f}}^*}{\varepsilon_{\mathrm{p}}^* + 2\varepsilon_{\mathrm{f}}^*}\right)\\ &= \frac{w^2(\varepsilon_{\mathrm{p}} - \varepsilon_{\mathrm{f}})(\varepsilon_{\mathrm{p}} + 2\varepsilon_{\mathrm{f}}) + (\sigma_{\mathrm{p}} - \sigma_{\mathrm{f}})(\sigma_{\mathrm{p}} + 2\sigma_{\mathrm{f}})}{w^2(\varepsilon_{\mathrm{p}} + 2\varepsilon_{\mathrm{f}})^2 + (\sigma_{\mathrm{p}} + 2\sigma_{\mathrm{f}})^2}\end{aligned} \tag{7}$$

The effective gravity expression is shown in Eq. (8).

$$F_{\mathrm{G}} = \frac{\pi d_{\mathrm{p}}^3(\rho_{\mathrm{p}} - \rho_{\mathrm{f}})g}{6\rho_{\mathrm{p}}} \tag{8}$$

where g is the gravitational constant, ρ_{p} is the particle density with a value of 1030 kg/m^3, and ρ_{f} is the density of the heat conducting oil with a value of 890 kg/m^3.

The expression for the drag force on a particle of diameter d_{p} moving under the action of dielectrophoresis and gravity is shown as Eq. (9).

$$F_{\mathrm{SD}} = \frac{\pi d_{\mathrm{p}}^2\rho_{\mathrm{p}}}{6\tau_{\mathrm{p}}}m_{\mathrm{p}}(u - v) \tag{9}$$

where v is the velocity of the fluid and τ_{p} is the particle velocity response time. As the mixture is almost stationary in the separator, the Reynolds number is very low, $v \approx 0$, $\tau_{\mathrm{p}} = \rho_{\mathrm{p}}d_{\mathrm{p}}^2/18\mu$, and μ is the fluid dynamic viscosity, which is influenced by the frequency of the electric field and is approximately 0.07 Pa·S. Substituting into Eq. (9) gives Eq. (10).

$$F_{\mathrm{SD}} = 3\pi\mu d_{\mathrm{p}}u \tag{10}$$

As the particle is subject to gravity only in the y direction, substituting Eqs. (4) and (10) into Eq. (2) gives Eq. (11).

$$\frac{\pi d_{\mathrm{p}}^3}{4}\varepsilon_{\mathrm{f}}\mathrm{Re}[f_{\mathrm{CM}}(w)]\cdot\frac{\partial|E|^2}{\partial n} - 3\pi\mu d_{\mathrm{p}}u_n = m_{\mathrm{p}}\frac{\mathrm{d}u_n}{\mathrm{d}t} \tag{11}$$

where n denotes the x or z direction. Solve Eq. (11) to obtain Eq. (12).

$$u_n = \frac{\varepsilon_{\mathrm{f}}d_{\mathrm{p}}^2}{12\mu}\mathrm{Re}[f_{\mathrm{CM}}(w)]\cdot\frac{\partial|E|^2}{\partial n}\left(1 - \mathrm{e}^{\frac{-18\mu}{d_{\mathrm{p}}^2\rho_{\mathrm{f}}}t}\right) \tag{12}$$

The experimental and simulation times used here are much greater than 10^{-6} s, such that $\mathrm{e}^{\frac{-18\mu}{d_{\mathrm{p}}^2\rho_{\mathrm{f}}}t} \approx 0$ and the particle in the xz plane of the velocity expression is shown in Eq. (13).

$$u_n = \frac{\varepsilon_{\mathrm{f}}d_{\mathrm{p}}^2}{12\mu}\mathrm{Re}[f_{\mathrm{CM}}(w)]\cdot\frac{\partial|E|^2}{\partial n} \tag{13}$$

Similarly, the expression for the velocity of a particle in the y direction under an alternating electric field can be obtained as Eq. (14).

$$u_y = -\left[\frac{\rho_{\mathrm{f}}g(\rho_{\mathrm{p}} - \rho_{\mathrm{f}})}{18\rho_{\mathrm{p}}} \pm \frac{\varepsilon_{\mathrm{f}}}{12}\mathrm{Re}[f_{\mathrm{CM}}(w)]\cdot\frac{\partial|E|^2}{\partial y}\right]\cdot\frac{d_{\mathrm{p}}^2}{\mu} \tag{14}$$

3. Analysis of the experiments and simulations

3.1. Characterization of AC-DEP behaviour of particles

The electrical performance parameters of each substance at room temperature are shown in Table 2.

The dielectric constant ε and the relative dielectric constant ε_{r} meet $\varepsilon = \varepsilon_0\cdot\varepsilon_{\mathrm{r}}$, where ε_0 is the vacuum dielectric constant, which has a value of approximately 8.854×10^{-12} F/m. $\mathrm{Re}[f_{\mathrm{CM}}(w)]$ directly determines the direction of the dielectrophoretic force on the particles. The frequency response characteristic curves of catalyst particles in the thermal oil and FCCS oil phases calculated by Eq. (7) are shown in Fig. 4, $\mathrm{Re}[f_{\mathrm{CM}}(w)] > 0$, so the particles are more strongly polarized and are always subject to positive dielectrophoretic forces (pDEP) in the separator. The catalyst particles will move in the direction of increasing electric field strength. For the two different oil phase systems, the calculated results of $\mathrm{Re}[f_{\mathrm{CM}}(w)]$ are close because the conductivity of the catalyst particles is much greater than that of the two oil phases. Although the oil phase media of the two systems are different, the influence of the electrophoretic force on the particles is minimal, which verifies the reliability of the cold model experiment using thermal oil preparation to simulate FCCS for particle removal.

Table 2
Electrical properties of each substance.

Items	Glass fillers	Zirconia fillers	Silicon carbide fillers	Heat conducting oil	FCCS oil phase	Catalyst particles
ε_r	5.82	19.50	8.60	1.46	1.43	6.22
σ, S/ m	1×10^{-16}	1×10^{-17}	1×10^{-7}	1.59×10^{-11}	1.90×10^{-11}	3.27×10^{-7}

Simulations using COMSOL provide results on the electric field intensity distribution and catalyst particle motion within the separation cell. The filler angle θ is chosen as 0° and 90°, and the excitation parameters for the applied square wave power supply are as follows: peak voltage $V_{pp} = 8$ kV, frequency $f = 10$ Hz, and duty cycle $q = 0.5$. The results obtained from the simulations for the *xoz* cross section at the moment of high and low level ($t = 4.3$ T and $t = 4.8$ T, respectively, T is the period of the alternating electric field) are shown in Fig. 5. For a more visual representation of the particle motion, the arrow tails are used to indicate the position of the particle in the separation cell, where the direction of the arrow indicates the direction of motion of the catalyst particles, and the color of the arrow indicates the potential value at the spatial point. Because the catalyst particles are mainly driven by the dielectrophoretic force, the arrow direction can also approximate the direction of the dielectrophoretic force. Under an alternating electric field, the electric field strength distribution within the separation cell remains constant as time changes, although the direction of the potential continues to change.

Regarding the contact point of the fillers at $\theta = 0°$, the nearby area is always a region of high electric field strength, and the particles move towards the contact point because of the pDEP. For comparison, the region near the contact point of the fillers with $\theta = 90°$ is a region of low electric field strength, where the particles move away from. The filler also has a relatively high electric field strength in the region near the positive and negative electrodes and can adsorb some of the particles, which is consistent with the experimental result that the inner electrode will adsorb some of the catalyst particles (Fig. 6).

Regarding the square wave power supply with peak voltage $V_{pp} = 8$ kV, $f = 40$ Hz, and $q = 0.5$, Fig. 7 shows the curve of the dielectrophoretic force on several particles over time at $\theta = 0°$. Due to the short simulation time and the small distance through which the particles move, the position of the particle in the space point is almost unchanged, and the field intensity gradient value of the

particle in the space point can be approximately regarded as the whole process value in this period. The dielectrophoretic force on the particles is always positive. In each half cycle, the direction of the potential changes, and there is a peak in the dielectric electrophoresis force of the particles. The dielectrophoretic force of the No.1 and No.2 particles is significantly greater than that of the No.3 and No.4 particles. This occurs because $f_{CM}(w)$ is constant under the condition of the same frequency electric field. At this time, the electric field gradient will directly affect the dielectrophoretic force. Fig. 5 shows that the electric field gradient near the contact point of the two fillers is significantly greater than that at other positions, so the particles will be subject to greater dielectrophoretic force.

3.2. "Effective contact points" under an alternating electric field

The area near the contact points between the fillers is the main area for the adsorption of catalyst particles. For the partition interface between the heat conducting oil and the filler, the electric flux density $\mathbf{D} = \varepsilon \cdot \mathbf{E}$. Assuming that there is no free surface charge density at the partition interface, the normal component of the electric flux density is continuous, thus giving Eqs. (13) and (14)

$$\mathbf{D}_{n,f} = \mathbf{D}_{n,g} \tag{13}$$

$$\varepsilon_f \cdot \mathbf{E}_{n,f} = \varepsilon_g \cdot \mathbf{E}_{n,g} \tag{14}$$

where $\mathbf{D}_{n,f}$ and $\mathbf{D}_{n,g}$ represent the electric flux densities near the heat conducting oil and near the filler at the partition, respectively. $\mathbf{E}_{n,f}$ and $\mathbf{E}_{n,g}$ denote the electric field intensity in the normal direction at the boundary between the adjacent mixture and the adjacent filler, respectively.

The electric field intensity at the partition interface meets Eq. (15) in the tangential component (Li et al., 2019).

$$\mathbf{E}_{t,f} = \mathbf{E}_{t,g} \tag{15}$$

where $\mathbf{E}_{t,f}$ and $\mathbf{E}_{t,g}$ represent the electric field intensity in the tangential direction near the boundary between the mixture and the filler, respectively.

Therefore, the electric field strength on the filler side at the intersection of the filler and the mixture can be derived as shown in Eq. (16).

$$\mathbf{E}_g = \sqrt{\mathbf{E}_{t,f}^2 + \left(\frac{\mathbf{E}_{n,f} \times \varepsilon_g}{\varepsilon_f} \right)^2} \tag{16}$$

Based on the basic principle of dielectric polarization, the expression for the depolarized electric field $\mathbf{E}'$ is given by Eq. (17)

$$\mathbf{E}' = \frac{\mathbf{P}}{3\varepsilon_{r,f}} \tag{17}$$

where $\mathbf{P}$ represents the intensity of polarization. Assuming that the packed sphere is an isotropic dielectric, the expression for $\mathbf{P}$ is shown in Eq. (18).
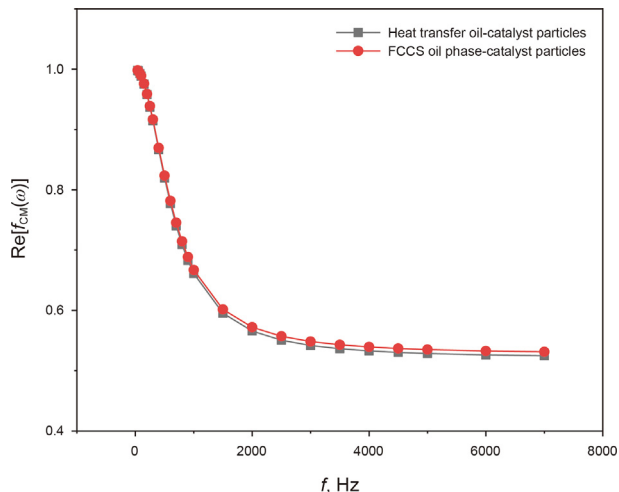

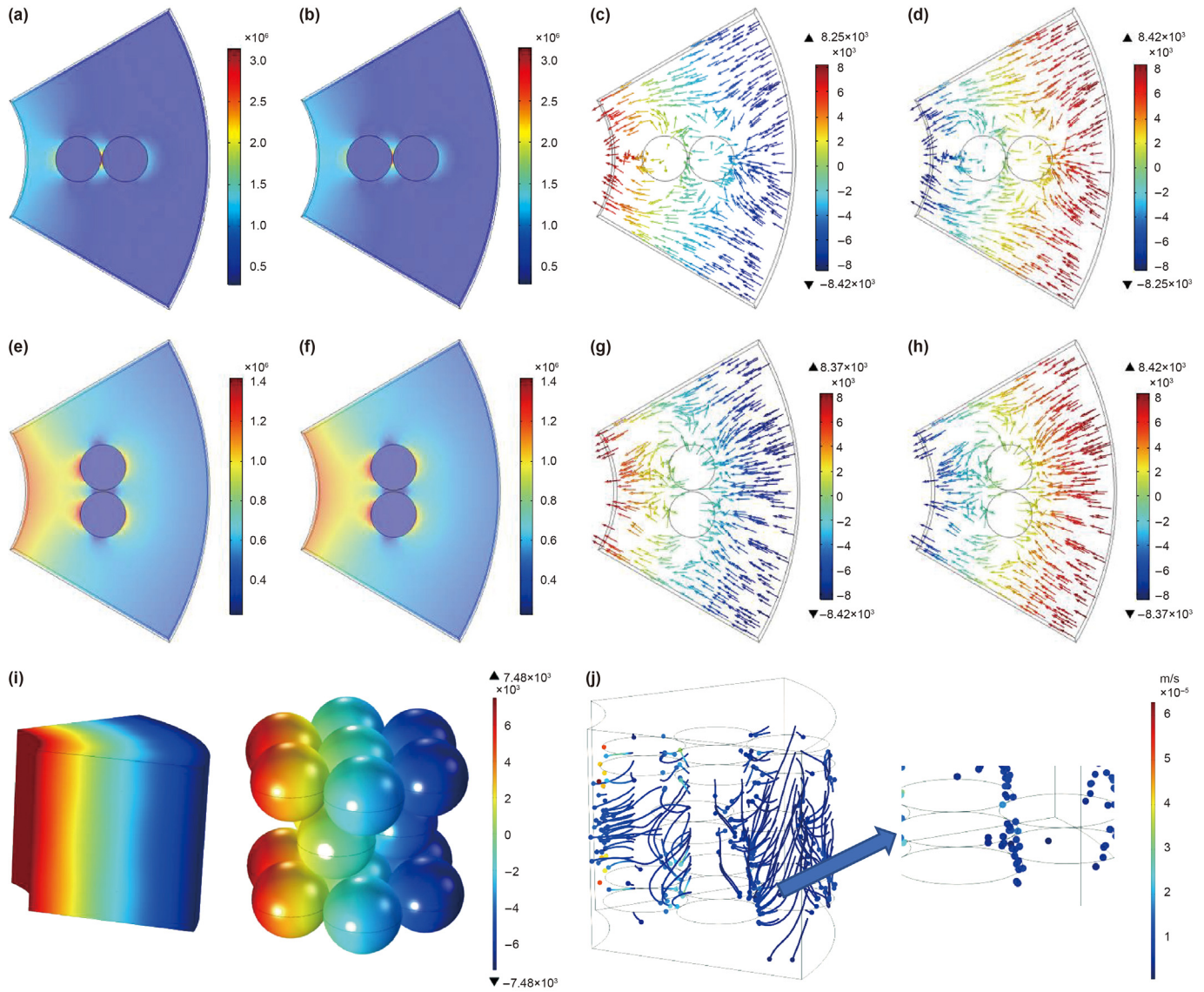**Fig. 4.** Frequency response characteristics of catalyst particles.

Fig. 5. Electric field strength at *xoz* cross and catalyst particle motion. **(a)** $\theta = 0°$, $t = 4.3$ T, electric field strength distribution; **(b)** $\theta = 0°$, $t = 4.8$ T, electric field strength distribution; **(c)** $\theta = 0°$, $t = 4.3$ T, movement of the particles; **(d)** $\theta = 0°$, $t = 4.8$ T, movement of the particles; **(e)** $\theta = 90°$, $t = 4.3$ T, electric field strength distribution; **(f)** $\theta = 90°$, $t = 4.8$ T, electric field strength distribution; **(g)** $\theta = 90°$, $t = 4.3$ T, movement of the particles; **(h)** $\theta = 90°$, $t = 4.8$ T, movement of the particles; **(i)** Electrical potential diagram of the separator and internal packing; **(j)** Particle trajectory diagram.

$$\mathbf{P} = \chi \varepsilon_{r,f} \mathbf{E} \tag{18}$$

where χ denotes the effective polarization rate and $\mathbf{E}$ denotes the strength of the electric field in the separation device. When spherical fillers with conductivity σ_g and dielectric constant ε_g are submerged in a liquid medium with conductivity σ_f and dielectric constant ε_f, the effective polarization rate of the spherical fillers under the action of an alternating electric field with frequency f is shown in Eq. (19).

$$\chi = a \cdot \frac{2\pi f \left(\varepsilon_g - \varepsilon_f \right) - i \left(\sigma_g - \sigma_f \right)}{2\pi f \left(\varepsilon_g + 2\varepsilon_f \right) - i \left(\sigma_g + 2\sigma_f \right)} \tag{19}$$

where a is a correction factor. The real part of χ is calculated as Eq. (20).

$$\mathrm{Re}(\chi) = a \cdot \frac{w^2 \left(\varepsilon_g - \varepsilon_f \right) \left(\varepsilon_g + 2\varepsilon_f \right) + \left(\sigma_g - \sigma_f \right) \left(\sigma_g + 2\sigma_f \right)}{w^2 \left(\varepsilon_g + 2\varepsilon_f \right)^2 + \left(\sigma_g + 2\sigma_f \right)^2} \tag{20}$$

We set the electric field generated by the power supply as $\mathbf{E}_0$ and the depolarization electric field as $\mathbf{E}'$. Because the fillers are isotropic linear dielectric and the directions of $\mathbf{E}_0$ and $\mathbf{E}'$ inside the fillers are opposite, the electric field intensity $\mathbf{E}$ in the separation device satisfies Eq. (21).

$$\mathbf{E} = \mathbf{E}_0 - \mathbf{E}' \tag{21}$$

The tangential component $\mathbf{E}_n$ and the normal component $\mathbf{E}_t$ of the electric field intensity inside the fillers can be obtained by simultaneous Eqs. (17), (18) and (21).
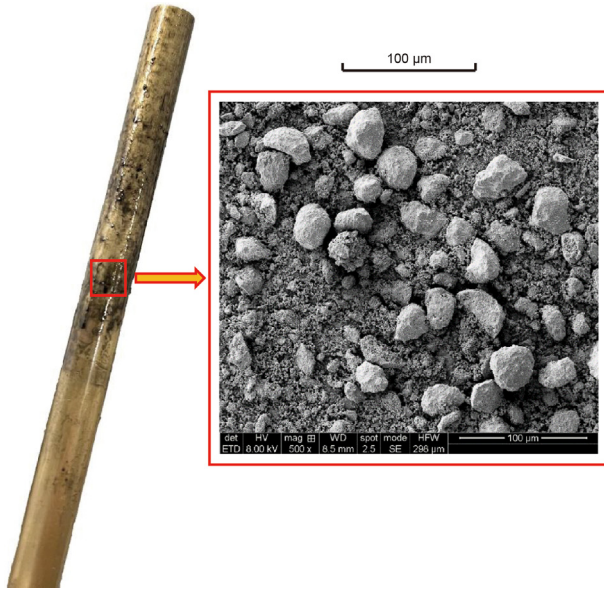
Fig. 6. Adsorption of catalytic particles by the inner electrode (the electrode surface is in contact with fillers at locations of high electric field strength, and the particle adsorption amount is large).
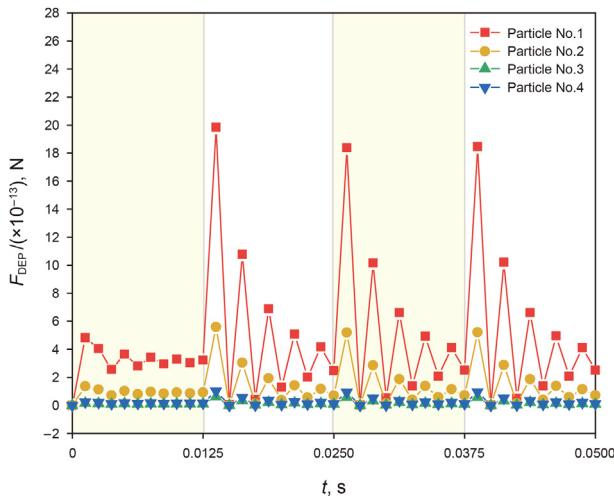

Fig. 7. Dielectrophoretic force on catalyst particles (No.1 and No.2 catalyst particles are released near the contact point of the filler, and the release coordinates are (0, 0.001, 0), (0, 0.001, 0.001); No.3 and No.4 catalyst particles are released far away from the contact point, and the release coordinates are (−0.001, 0, 0.004) and (−0.002, 0.001, −0.0035), respectively. The yellow area is the time period of high potential values.).

$$\mathbf{E}_n = \mathbf{E}\cos\theta = \frac{3E_0}{3 + \mathrm{Re}(\chi)}\cos\theta \tag{22}$$

$$\mathbf{E}_t = \mathbf{E}\sin\theta = \frac{3E_0}{3 + \mathrm{Re}(\chi)}\sin\theta \tag{23}$$

The simultaneous Eqs. (16), (22) and (23) give the relation between $\mathbf{E}_g$ and $\mathbf{E}_0$, as shown in Eq. (24).

$$\mathbf{E}_g = \frac{3\sqrt{\varepsilon_{r,f}^2 + \left(\varepsilon_{r,g}^2 - \varepsilon_{r,f}^2\right)\cos^2\theta}}{(3 + \mathrm{Re}(\chi))\varepsilon_{r,f}}\mathbf{E}_0 \tag{24}$$

The dimensionless number α is defined to characterize the expansion of the original electric field after the polarization of the separated region. The expression of α is expressed as Eq. (25).

$$\alpha = \frac{\mathbf{E}_g}{\mathbf{E}_0} = \frac{3\sqrt{\varepsilon_{r,f}^2 + \left(\varepsilon_{r,g}^2 - \varepsilon_{r,f}^2\right)\cos^2\theta}}{(3 + \mathrm{Re}(\chi))\varepsilon_{r,f}} \tag{25}$$

The effective contact point model under an alternating electric field suggests that the electrical properties of the filler, the filler angle θ, and the electric field frequency f affect the electric field strength and the direction of the electric field gradient at the contact point of the filler, which in turn affects the adsorption of the catalyst particles at the contact point of the filler. To verify the accuracy of Eq. (25), the correction factor a was neglected, and the separation unit of Fig. 3 was selected for calculation. Taking a square wave power excitation with a voltage amplitude of 8 kV as an example, the materials of the filler were selected as glass, zirconia and silicon carbide, and the calculated $\mathrm{Re}(\chi)$-f curve is shown in Fig. 8. The difference in the $\mathrm{Re}(\chi)$ between silicon carbide and the other two fillers is due to its high conductivity. The calculated results for α are shown in Fig. 9.

From the results of the effective contact point model in Fig. 9, the value of α decreases as the angle θ increases, which will be detrimental to the adsorption of catalyst particles at the contact point. θ affects the magnitude of the contact point to the original electric field, which in turn affects the direction of the electric field intensity gradient and F_{DEP}. When $\alpha = 1$, the field strength of the contact point is essentially unaffected by the polarization of the filler. When the filler angle θ is small and $\alpha > 1$, the contact point is a region of high electric field strength and can adsorb catalyst particles, i.e., the "effective contact point." The frequency of the electric field also affects the value of α. When using fillers with very low conductivity (glass and zirconia), the electric field frequency has almost no effect on the value of α, but when using fillers with a larger electrical conductivity (silicon carbide), with the increase of f, α first increases and then remains constant, it is clear for the contact points with a smaller θ and makes the electric field strength gradient at the contact points have the same trend. At the same time, it can be seen from Eq. (4) that the catalyst particles will be subject to greater dielectrophoretic force, and the contact points have a better adsorption effect on the particles.

To verify the variation in α with θ in the effective contact point model under an alternating electric field, microscopic experiments
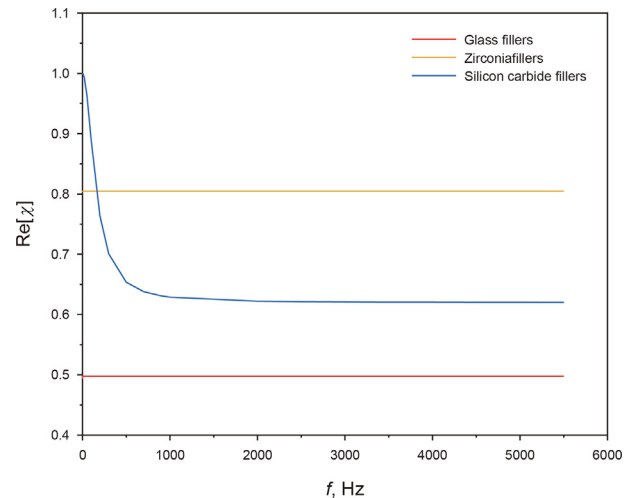

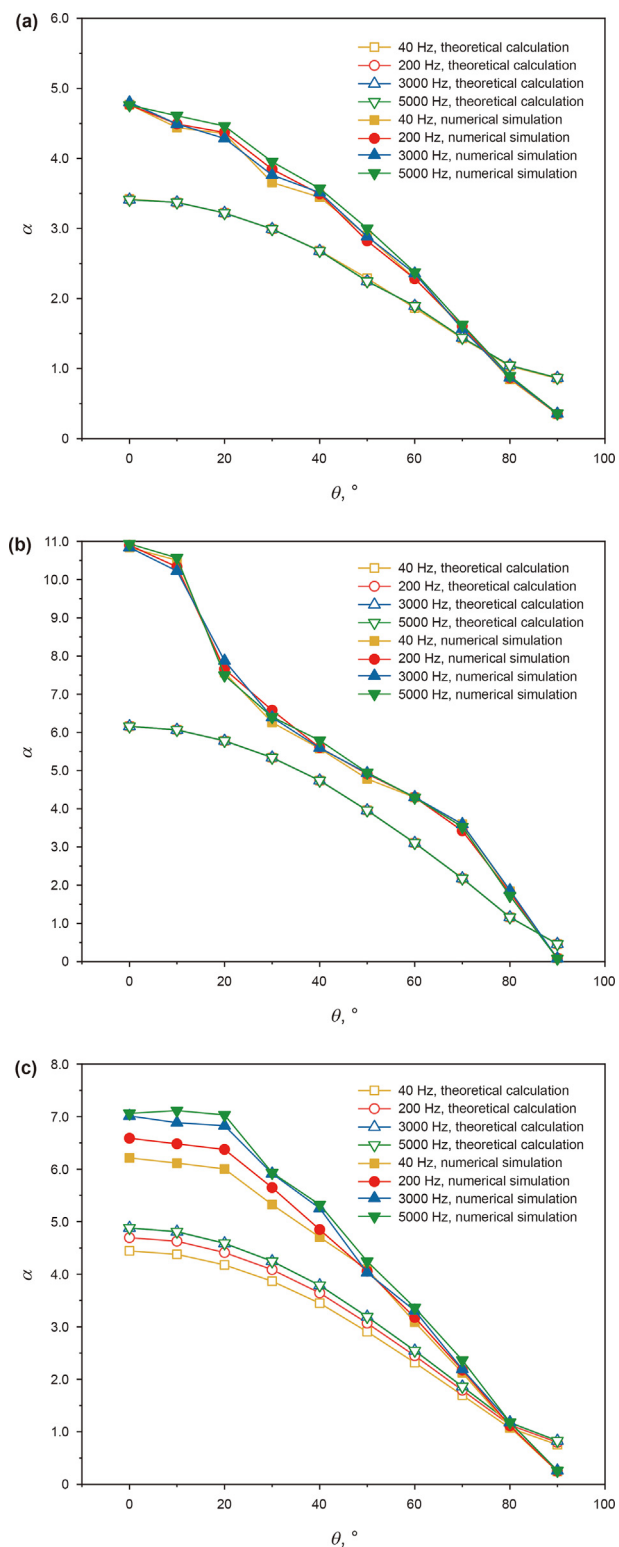**Fig. 8.** Calculation results for $\mathrm{Re}(\chi)$ at different f.

Fig. 9. Effective contact point model calculation. **(a)** Glass fillers; **(b)** Zirconia fillers; **(c)** Silicon carbide fillers.

Fig. 10. Particle adsorption. **(a)** Glass fillers; **(b)** Zirconia fillers; **(c)** Silicon carbide fillers.

Table 3
θ-values for contact points.

Items	A	B	C	D	E	F	G	H	I
θ, °	15.6	71.3	43.2	34.3	23.5	86.2	53.2	4.8	59.5

on the adsorption of catalyst particles were carried out. The adsorption of catalyst particles under a square electric field of $V_{pp} = 8$ kV, $q = 0.5$, and $f = 50$ Hz for 120 min was observed microscopically, as shown in Fig. 10. In Fig. 10, the direction of the alternating electric field is along the x-axis, and the θ values of the
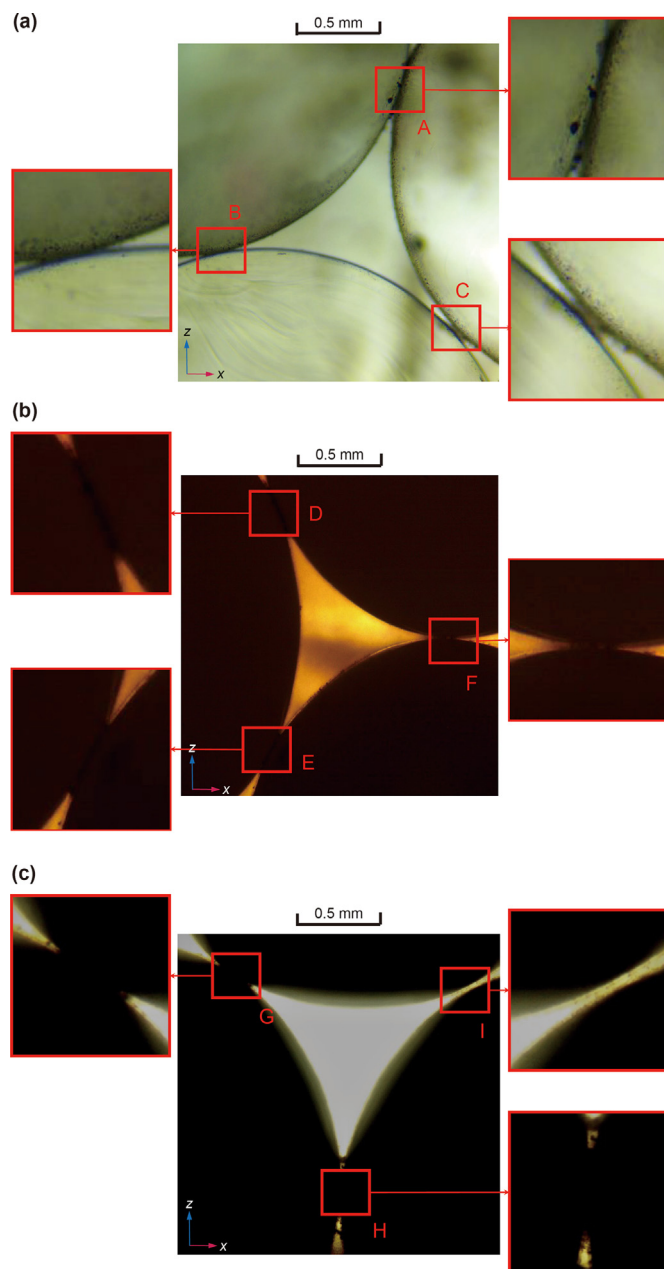
contact points are indicated in Table 3. The data show that there is very little adsorption at locations other than the contact points, which is consistent with the analysis of particle motion in Section 3.1 and indicates that the filler adsorbed particles retain "point adsorption" under alternating electric fields. Because the dielectrophoretic force is the main driving force for particle adsorption and the dielectrophoretic force on the particles is positively correlated with α, the adsorption of catalyst particles at the contact
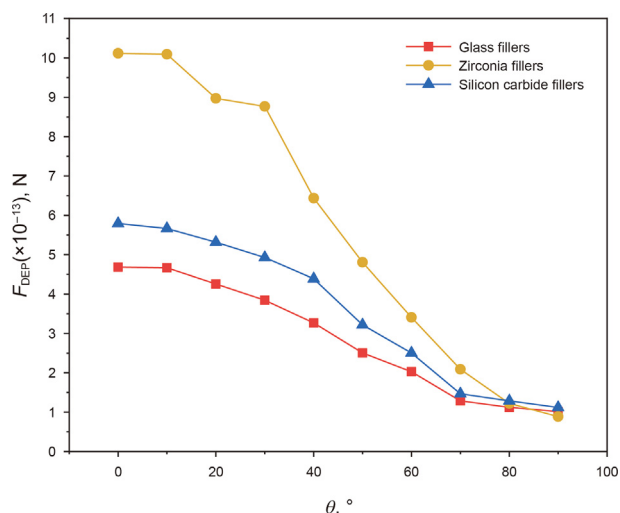
Fig. 11. Average dielectrophoretic force on particles at different θ (4 particles released near the contact point at different θ with release coordinates (0, 0.001, 0), (0, 0.001, 0), (0.001 sin θ, 0, 0.001 cos θ), (−0.001 sin θ, 0, 0.001 cos θ)).

Fig. 13. Variation of the dielectrophoretic force on the particles with f when using different fillers.

point is assumed to be positively correlated with α under the same conditions. In Fig. 10, the adsorption of catalyst particles in the region near the contact point satisfies an inverse relationship with the angle θ, which is consistent with the calculated results in Fig. 9. Simulations were carried out to calculate the numerical magnitude of the dielectrophoretic forces on the particles near the contact points at different θ under the same conditions, as shown in Fig. 11. In the simulation results of Fig. 11, the average dielectrophoretic force on the particles decreases with increasing θ, which also verifies the calculation results of the effective contact point model in Fig. 9.

To verify the effect of f on α in the effective contact point model, separate macroscopic separation experiments were carried out using the three fillers. The applied power excitation was a square wave with $V_{\mathrm{pp}} = 8$ kV and $q = 0.5$, and the experimental results obtained for different f are shown in Fig. 12. The numerical magnitude of the average dielectrophoretic force on the particles near the contact point was simulated in different f (Fig. 13). In the macroscopic separation experiments, the fillers dumped into the separator exhibited mainly hexagonal close packing (hcp) (Guo
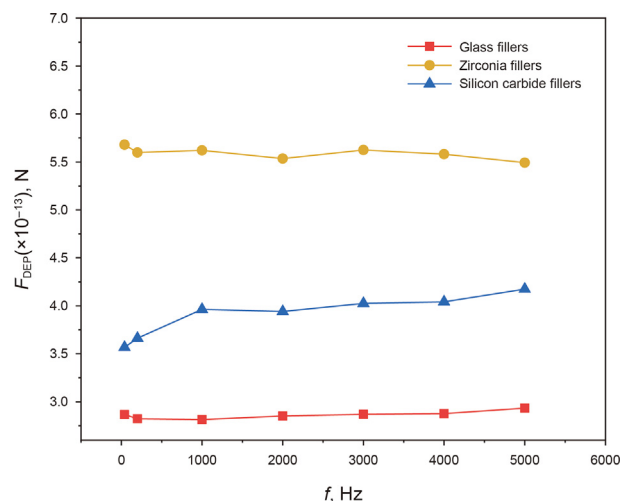
et al., 2017) due to the same diameter of each packing, so it can be assumed that the distribution of the number of various θ was fixed for each experiment. As shown in Fig. 12, when using glass fillers and zirconia fillers, the particle adsorption effect is not sensitive to the change in alternating electric field frequency (maximum variation of 17.61%). However, when using silicon carbide fillers, increasing the electric field frequency in the low-frequency band below approximately 2000 Hz resulted in a significant increase in adsorption efficiency (maximum variation of 44.97%), and when the electric field frequency exceeded 2000 Hz, the change in adsorption efficiency did not fluctuate significantly (maximum variation of 9.08%). Since the adsorption effect of contact points with large θ values on particles is weak, the increase in adsorption efficiency comes mainly from the low θ contact points, and the dielectrophoretic force is the main driving force in the process of particles being adsorbed. The results in Figs. 12 and 13 validate the effect of f on α in Fig. 9.

4. Conclusion

In this study, the electric field distribution and particle motion patterns in the separation unit of the FCCS particle removal process under an alternating electric field were obtained. Microscopic and macroscopic experiments were carried out to obtain the effects of the electric field frequency and filler parameters on the particle separation effect. An effective contact point model under an alternating electric field is proposed as $\alpha = \frac{3\sqrt{\varepsilon_{r,f}^2 + (\varepsilon_{r,g}^2 - \varepsilon_{r,f}^2)\cos^2\theta}}{(3 + \mathrm{Re}(\chi))\varepsilon_{r,f}}$, which illustrates that the electrical properties of the fillers, the fillers' angle θ, and the electric field frequency f affect the adsorption effect of the contact points, and the model is verified by corresponding simulations and experiments. When θ is approximately 0−75° and $\alpha > 1$, the contact point is a region of high electric field strength where the catalyst particles can be adsorbed, i.e., the effective contact point. When low conductivity fillers are selected (e.g., glass and zirconia fillers), the maximum change in α is only 17.61% when f increases from 40 to 5000 Hz. When a high-conductivity filler (e.g., silicon carbide filler) is selected, α increases significantly with increasing f, the maximum change rate is 44.97%, and then α remains stable. In a practical separation process, the electric field frequency can be tuned to a specific electric field frequency to achieve better adsorption by optimizing the combined effects of the electric field frequency on α and the viscosity of FCCS.
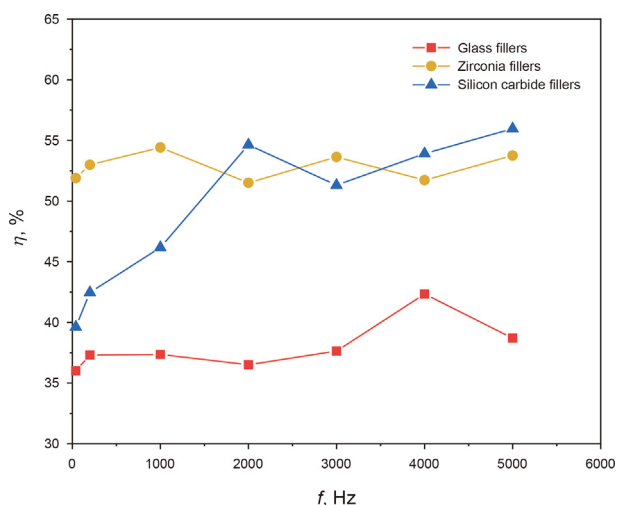

Fig. 12. The variation in η with f when using different fillers.

CRediT authorship contribution statement

Qiang Li: Conceptualization, Data curation, Formal analysis, Funding acquisition, Investigation, Methodology, Project administration, Software. **Hui-Zhen Yang:** Methodology, Project administration, Writing − original draft. **Can Yang:** Formal analysis, Project administration. **Qing-Zhu Qiu:** Formal analysis, Software. **Wei-Wei Xu:** Investigation, Software. **Zhao-Zeng Liu:** Visualization, Writing − review & editing.

Declaration of competing interest

The authors declare that they have no known competing financial interests or personal relationships that could have appeared to influence the work reported in this paper.

Acknowledgements

Appendix A. Supplementary data

Supplementary data to this article can be found online at https://doi.org/10.1016/j.petsci.2023.12.003.

References

Adekanmbi, E.O., Giduthuri, A.T., Srivastava, S.K., 2020. Dielectric Characterization and separation optimization of infiltrating ductal adenocarcinoma via insulator-dielectrophoresis. Micromachines 11 (4), 340. https://doi.org/10.3390/mi11040340.

Aldaeus, F., Lin, Y., Amberg, G., et al., 2006. Multi-step dielectrophoresis for separation of particles. J. Chromatogr. A. 1131 (1–2), 261–266. https://doi.org/10.1016/j.chroma.2006.07.022.

Cao, Q., Xie, X.L., Li, J.P., et al., 2011. A novel method for removing quinoline insolubles and ash in coal tar pitch using electrostatic fields. Fuel 96, 314–318. https://doi.org/10.1016/j.fuel.2011.12.061.

Chevron Research Company, 1979. Electrofiltration with Bi-directional Potential Pretreatment. US Patent, 19780876590.

Corporation, Petrolite, 1980. Media Regeneration in Electrofiltration. US Patent, 19780924464.

Cui, L.R., Chen, H., Xu, J., et al., 2020. Chemical modification process of heavy residue from FCC slurry oil for producing high-grade paving asphalt. Fuel 265, 117002. https://doi.org/10.1016/j.fuel.2019.117002.

Gulf Research & Development Company, 1975. Electrofilter. US Patent, 19740500476.

Fang, Y.J., Xiao, W.D., Wang, G.R., 1998. Study on electrostatic separation of solid-liquid system II. Measurement of saturated adsorption weight. Petrochem. Technol. 27 (11), 35−39 (in Chinese).

Guo, A.J., Wei, Z.X., Zhao, B., et al., 2014. Separation of toluene-insoluble solids in the slurry oil from a residual fluidized catalytic cracking unit: determination of the solid content and sequential selective separation of solid components. Energy Fuels 8 (5), 1452−1454. https://doi.org/10.1021/ef500353z.

Guo, A.J., Gong, L.M., Zhao, N., et al., 2017. The influence of additive modification on electrostatic separation of FCC slurry oil. Chem. Ind. Eng. Prog. 36 (9), 3266−3272. https://doi.org/10.16085/j.issn.1000-6613.2017-0093 (in Chinese).

Kuznetsov, N.M., Kovaleva, V.V., Belousov, S.I., et al., 2022. Electrorheological fluids: from historical retrospective to recent trends. Mater. Today Chem. 26, 101066. https://doi.org/10.1016/j.mtchem.2022.101066.

Lewpiriyawong, N., Xu, G.L., Yang, C., 2017. Enhanced cell trapping throughput using DC-biased AC electric field in a dielectrophoresis-based fluidic device with densely packed silica beads. Electrophoresis 39 (5−6), 878−886. https://doi.org/10.1002/elps.201700395.

Li, W.D., Chen, Y.L., Zhang, L.Z., et al., 2016. Supercritical fluid extraction of fluid catalytic cracking slurry oil: bulk property and molecular composition of narrow fractions. Energy Fuels 30 (12), 10064−10071. https://doi.org/10.1021/acs.energyfuels.6b01132.

Li, Q., Zhang, Z., Wu, Z.Z., et al., 2019. Effects of electrostatic field and operating parameters on removing catalytic particles from FCCS. Powder Technol. 342, 817−828. https://doi.org/10.1016/j.powtec.2018.10.060.

Li, Q., Li, A.M., Guo, L.F., et al., 2020a. Microscopic mechanistic study on the removal of catalyst particles in FCCS by an electrostatic field. Powder Technol. 363, 500−508. https://doi.org/10.1016/j.powtec.2020.01.019.

Li, Q., Guo, L.F., Cao, H., et al., 2020b. Effects of an effective adsorption region on removing catalyst particles from an FCC slurry under a DC electrostatic field. Powder Technol. 377, 676−683. https://doi.org/10.1016/j.powtec.2020.09.038.

Liang, Y.D., Huang, D.Y., Zhou, X.F., et al., 2022. Efficient electrorheological technology for materials, energy, and mechanical engineering: from mechanisms to applications. Engineering 24, 151−171. https://doi.org/10.1016/j.eng.2022.01.014.

Lin, I.J., Benguigui, L., 1981. Dielectrophoretic filtration and separation: general outlook. Separ. Purif. Methods 10 (1), 53−72. https://doi.org/10.1080/03602548108066007.

Lin, I.J., Benguigui, L., 1982. Dielectrophoretic filtration of liquids. II. Conducting liquids. Separ. Sci. Technol. 17 (5), 645−654. https://doi.org/10.1080/01496398208068557.

Lou, B., Liu, D., Qiu, Y., et al., 2021. Modified effect on properties of mesophase pitch prepared from various two-stage thermotreatments of FCC decant oil. Fuel 284 (21), 119034. https://doi.org/10.1016/j.fuel.2020.119034.

Mazumder, M.K., Sims, R.A., Biris, A.S., et al., 2005. Twenty-first century research needs in electrostatic processes applied to industry and medicine. Chem. Eng. Sci. 61 (7), 2192−2211. https://doi.org/10.1016/j.ces.2005.05.002.

Murugesan, R., Park, J.H., 2017. Electrophoretic and dielectrophoretic trapping of molecular objects in planar quadrupole electrode configuration at room temperature. J. Mech. Sci. Technol. 31 (3), 1331−1339. https://doi.org/10.1007/s12206-017-0233-y.

Sano, N., Matsukura, B., Ikeyama, Y., et al., 2012. Dielectrophoretic particle separator using mesh stacked electrodes and simplified model for multistage separation. Chem. Eng. Sci. 84, 345−350. https://doi.org/10.1016/j.ces.2012.08.034.

Wu, H.B., Wen, J., Zhang, L.H., et al., 2020. Purification of catalytic cracking slurry and comprehensive utilization to produce high value-added products, 2635 Appl. Chem. Ind. 49 (10), 2618−2624. https://doi.org/10.16581/j.cnki.issn1671-3206.20200724.014 (in Chinese).

Xie, Y.W., Li, H.Y., Huang, Q., et al., 2023a. The mechanism of viscosity reduction of waxy oils induced by the electric field: a correlation between the viscosity reduction and the charged particle accumulation on wax particles. J. Colloid Interface Sci. 642, 373−379. https://doi.org/10.1016/j.jcis.2023.03.171.

Xie, Y.W., Li, H.Y., Zhang, C.Y., et al., 2023b. A further investigation to mechanism of the electrorheological effect of waxy oils: behaviors of charged particles under electric field. Petrol. Sci. 20 (2), 1247−1254. https://doi.org/10.1016/j.petsci.2022.08.022.

Xie, Y.W., Li, H.Y., Xu, M.M., et al., 2023c. Effect of shear on durability of viscosity reduction of electrically-treated waxy crude oils. Energy 284, 128605. https://doi.org/10.1016/j.energy.2023.128605.